Large scale biomimetic membrane arrays

ARTICLE *in* ANALYTICAL AND BIOANALYTICAL CHEMISTRY · SEPTEMBER 2009

Impact Factor: 3.44 · DOI: 10.1007/s00216-009-3010-7 · Source: PubMed

10 AUTHORS, INCLUDING:

Jörg Vogel

8 PUBLICATIONS **99** CITATIONS

SEE PROFILE

Marianne S Larsen

3 PUBLICATIONS **28** CITATIONS

SEE PROFILE

Henrik Bohr

Technical University of Denmark

140 PUBLICATIONS **2,711** CITATIONS

SEE PROFILE

Claus Helix-Nielsen

Technical University of Denmark

84 PUBLICATIONS **1,740** CITATIONS

SEE PROFILE

Anal Bioanal Chem (2009) 395:719–727
DOI 10.1007/s00216-009-3010-7

ORIGINAL PAPER

Large scale biomimetic membrane arrays

Jesper S. Hansen · Mark Perry · Jörg Vogel · Jesper S. Groth · Thomas Vissing · Marianne S. Larsen · Oliver Geschke · Jenny Emneús · Henrik Bohr · Claus H. Nielsen

Received: 2 July 2009 / Revised: 22 July 2009 / Accepted: 23 July 2009 / Published online: 13 August 2009

Abstract To establish planar biomimetic membranes across large scale partition aperture arrays, we created a disposable single-use horizontal chamber design that supports combined optical–electrical measurements. Functional lipid bilayers could easily and efficiently be established across CO_2 laser micro-structured 8×8 aperture partition arrays with average aperture diameters of 301±5 μm. We addressed the electro-physical properties of the lipid bilayers established across the micro-structured scaffold arrays by controllable reconstitution of biotechnological and physiological relevant membrane peptides and proteins. Next, we tested the scalability of the biomimetic membrane design by establishing lipid bilayers in rectangular 24×24 and hexagonal 24×27 aperture arrays, respectively. The results presented show that the design is suitable for further developments of sensitive biosensor assays, and furthermore demonstrate that the design can conveniently be scaled up to support planar lipid bilayers in large square-centimeter partition arrays.

J. S. Hansen · J. Vogel · O. Geschke · J. Emneús
DTU Nanotech, Technical University of Denmark,
2800 Lyngby, Denmark

J. S. Hansen
e-mail: jsh@aquaporin.dk

J. S. Hansen · M. Perry · J. Vogel · J. S. Groth · T. Vissing · M. S. Larsen · C. H. Nielsen
Aquaporin A/S, Scion DTU,
Diplomvej 377,
2800 Lyngby, Denmark

H. Bohr · C. H. Nielsen (✉)
DTU Physics, Quantum Protein Center,
Technical University of Denmark,
2800 Lyngby, Denmark
e-mail: claus.nielsen@fysik.dtu.dk

Keywords Black lipid membrane · Array · Optical–electrical measurements · Membrane-spanning peptides · Membrane protein

Abbreviations

α-HL	α-Hemolysin
BLM	Black lipid membrane
DPhPC	1,2-Diphytanoyl-*sn*-Glycero-3-Phosphocholine
ETFE	Ethylene tetrafluoroethylene
FomA	*Fusobacterium nucleatum* outer membrane protein A
gA	Gramicidin A
LDAO	*N*-lauryl-*N*,*N*-dimethylammonium-*N*-oxide
NBD-PC	1-Oleoyl-2-[6-[(7-nitro-2-1, 3-benzoxadiazol-4-yl)amino]hexanoyl]-*sn*-glycero-3-phosphocholine
TEA	Tetraethylammonium

Introduction

To create a device that utilizes membrane-spanning molecules, it is necessary to construct an efficient platform to handle biomimetic membranes [1]. The advantages of biomimetic membrane-based applications are, among others, that a lot of information can be achieved with extremely low sample volumes, specific drug interactions with a single target (protein or peptide) can be assessed, and the experimental conditions can be exactly controlled (e.g., buffer, protein amount, and membrane composition) [1].

Biomimetic membrane-based biosensing devices may provide a powerful tool in the early stage of identifying promising drug candidates for a specific membrane protein or peptide [2–5]. Moreover, a reduction in drug candidates

failing at later stages may be expected. The reason for this is the ability to exactly address the specific effects of a drug candidate on a single target, as well as the potential unintended effects that may occur due to the physiochemical properties of the lipid membrane [6]. This reduces the potential of obtaining unintended interactions with secondary receptors or proteins, or potentially indirect effects on the lipid membrane, which may otherwise occur in living-cell-based systems.

Recently, we described a fast and cost efficient method to produce large scale aperture partitions by micro-structuring ethylene tetrafluoroethylene (ETFE) films using CO_2 laser ablation [7]. In a parallel study, we constructed a vertical automation technique for the simultaneous establishment of functional bilayers in 8×8 partition arrays [8].

In this study, we created a horizontal biomimetic membrane design supporting optical–electrical measurements of lipid bilayers established across the CO_2 laser-ablated ETFE LZ200 partition arrays. The chamber design was created to constitute a low-cost disposable single-use system. Lipid bilayers could efficiently be established across the partition arrays in the chamber design by employing a modified painting method [9]. The success rate for establishing lipid bilayers across the partition array in the presented design was ≥98%. To demonstrate the functionality of the biomimetic membrane design, controllable reconstitution of the biotechnological and physiological relevant peptides valinomycin and gramicidin A (gA), together with the membrane proteins α-hemolysin and FomA was carried out. We show that the design supports low-current (high sensitivity) recordings of membrane peptides and proteins by incorporating gA, α-hemolysin, and FomA into the established lipid bilayers.

Finally, we demonstrate that the design can conveniently be scaled up to 24×24 (576 apertures) rectangular and 24×27 (648 apertures) hexagonal membrane arrays with averaged diameters of 300 μm. The two different geometries of the micro-structured aperture arrays seem to support stable membrane arrays, however, with somewhat different electrical properties.

Our results are discussed in the context of improving the design to create a multifunctional biomimetic platform suitable for the development of biosensing devices.

Experimental

Reagent and materials

Tefzel ETFE LZ200 fluoropolymer for the fabrication of multi-aperture partitions, and Viton A fluoroelastomer for the production of rubber chamber sealing rings were from DuPont Fluoropolymers (Detroit, U.S.A.). Uncoated 35- and 50-mm glass-bottom culture dishes were purchased from MatTek Corporation (Ashland, MA, U.S.A.). The lipids 1, 2-diphytanoyl-*sn*-glycero-3-phosphocholine and 1-oleoyl-2-[6-[(7-nitro-2-1, 3-benzoxadiazol-4-yl)amino]hexanoyl]-*sn*-glycero-3-phosphocholine were from Avanti Polar Lipids Inc. (Alabaster, U.S.A.). The potassium ion-selective cyclodepsipeptide valinomycin (Sigma), *Bacillus brevis* gramicidin A (Sigma), *Staphylococcus aureus* α-Hemolysin (Sigma), tetraethylammonium (Fluka), *n*-heptane and *n*-decane (Fluka) were purchased from Sigma-Aldrich Denmark (Brøndby, Denmark). All other chemicals were of analytical grade and purchased from commercial sources.

Micro-structuring and surface modification of ETFE scaffold arrays

ETFE LZ200 film (50.8 μm thickness) was laser-structured to produce partition aperture arrays as previously described [7]. Partitions produced were rectangular 8×8 and 24×24, and hexagonal 24×27 arrays, respectively. The apertures within the partition structure had average diameters of 301±5 μm and with a nominal distance from center-to-center of 400 μm.

The ETFE surfaces were covalently modified by plasma treatment with lower-carbon-chain-length alkanes, predominantly hexanes, resulting in a hydrophobic surface coating as described by Inagaki et al. [10] and by Park and Inagaki [11]. This surface modification was applied to provide a molecular anchoring for establishing the lipid membranes across the micro-structured arrays.

Disposable single-use horizontal biomimetic membrane chamber design

A horizontal lipid bilayer chamber was designed for optical imaging that at the same time enabled recording of the electrical membrane properties by voltage clamp. The assembly of the chamber design is schematically depicted in Fig. 1a. The design was inspired from previous work by Hemmler et al. [12] and Wilburn et al. [13], respectively. Our chamber was, however, made from commercially available 35- and 50-mm MatTek glass-bottom culture dishes, where the 35-mm dish constituted the upper and the 50-mm dish the lower compartments, respectively (Fig. 1). The glass cover slip of the 35-mm MatTek glass-bottom dishes was replaced with the ETFE LZ200 partition by first removing the cover slip by adding 0.5 ml *n*-heptane to the dishes for 10 min, and then gluing the ETFE LZ200 partition array on the dish using silicone-based glue (Dow Corning). A reusable aluminum microscope sample holder was designed to clamp the upper and lower compartments (Fig. 1b and c). A 34-mm cut Viton ring was placed between the two Petri dishes to create two independently accessible compartments (Fig. 1c). By design, the chamber components were made of low-cost, commercially available

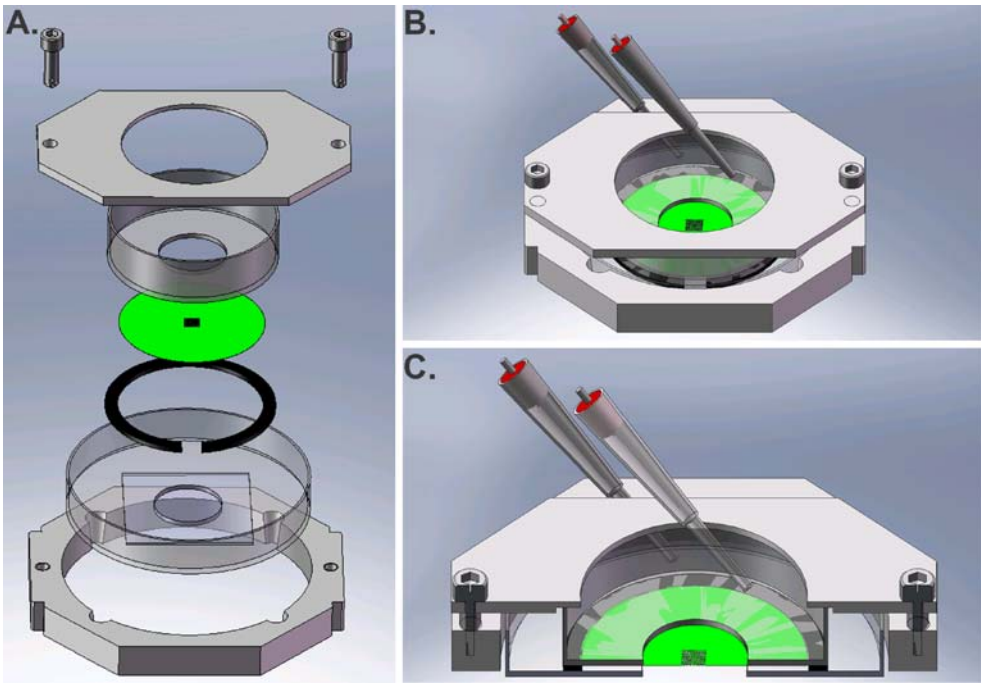

Fig. 1 The horizontal lipid chamber design. **a** Assembly of the bilayer chamber. The chamber is assembled sequentially from the bottom and up. The upper *cis* compartment consists of a MatTek 35 mm culture dish (transparent) with a micro-structured ETFE LZ200 partition (*green*) glued onto the bottom across the center hole. A MatTek 50-mm-diameter glass-bottom culture dish constitutes the lower *trans* compartment (*transparent*). A cut Viton ring (*black*) is placed between the dishes to create two independently accessible compartments. A custom-designed aluminum sample holder clamps the chamber elements together (*gray*). **b** The assembled lipid chamber. **c** Cross-sectional view of the assembled chamber. The position of the Ag/AgCl electrodes connected to the voltage-clamp setup is indicated in **b** and **c**

components that constituted a convenient disposable single-use chamber design.

Preparation of lipid solutions for BLM experiments

The lipid solution for bilayer formation consisted of 1, 2-diphytanoyl-*sn*-glycero-3-phosphocholine (DPhPC) in *n*-decane (25 mg/ml) doped with 1 mol% 1-oleoyl-2-[6-[(7-nitro-2-1, 3-benzoxadiazol-4-yl)amino]hexanoyl]-*sn*-glycero-3-phosphocholine (NBD-PC). The lipid solution for bilayer formation is henceforth referred to as the bilayer-forming solution (BFS). The lipid solutions were prepared the day before, and stored at −20°C until use.

Formation of BLMs across multi-aperture ETFE partitions

Planar lipid bilayers were established across the micro-structured ETFE partition arrays by the lipid bilayer painting technique [9], which was modified essentially, as previously described [12]. Briefly, ~0.5–5 µl (depending on the array size) of the BFS was deposited onto the partition array. To thin the membranes into bilayers, a sterile plastic inoculation loop with a 1 µl loop capacity (Sarstedt) was used. The thinning process was carried out by gently sweeping the inoculation loop across the entire ETFE partition array.

Fluorescence microscopy visualization

Fluorescent imaging was performed on a Zeiss Axiovert 200M epifluorescence microscope (Carl Zeiss, Jena, Germany) equipped with a monochrome Deltapix DP450 CCD camera (Deltapix, Maalov, Denmark). Images were acquired using Deltapix DpxView Pro acquisition software (Deltapix, Maalov, Denmark). Objectives used were air-corrected Plan-Neofluar 2.5×/0.075 Numerical Aperture (NA) and 10×/0.25 NA, respectively.

Voltage-clamp data acquisition and processing

The experimental setup consisted of a Model 2400 Patch Clamp Amplifier with a head stage containing 10 GΩ/10 MΩ feedback resistors (A-M Systems, Inc., WA, USA) and a Thurlby Thandar Instruments model TG2000 20 MHz DDS function generator (RS Components Ltd, Northants, UK). The Ag/AgCl electrodes were placed in the *trans* and *cis* compartments of the bilayer formation chamber with the ground electrode positioned in the *trans* compartment. Data acquisition was done with a combined oscilloscope/analog–digital converter (ADC-212/50, Pico Technology, Cambridgeshire, UK) connected to a laptop computer. Sampling frequency was 50 Hz.

Capacitance and conductance measurements were performed as previously described [8]. The results are given as means±S.D. for five individual experiments unless otherwise stated. Off-line analysis was done using custom made software.

To measure channel incorporation electrically, a current potential of +60 mV or +150 mV was applied, and the resulting membrane output current was filtered through 1 kHz on the amplifier and subsequently further filtered through a low-pass Bessel filter with 50 Hz cutoff (Frequency Devices, IL, USA) before data acquisition.

Reconstitution of transmembrane peptides and proteins

Valinomycin dissolved in ethanol (1.8 mM) was added (10 µl) to the top horizontal chamber to yield a final concentration of 12 µM in close proximity to the lipid bilayer array. To reverse the valinomycin-induced current increase, tetraethylammonium (TEA, 16 mM) was added (200 µl) to the top horizontal chamber. The aqueous chamber solution consisted of 0.2 M KCl. The applied potential across the partition arrays was +60 mV.

Incorporation of *B. brevis* gramicidin A (gA) into established membrane arrays was carried out by the addition of 5 µl gA dissolved in ethanol (120 nM) to both the *cis* and *trans* horizontal chambers. The aqueous solution in the bilayer chamber consisted of HCl (1 N) adjusted to pH 1.0, while the potential applied across the bilayers was +150 mV.

S. aureus α-hemolysin (α-HL) was reconstituted into 8×8 bilayer arrays by adding 10 µl of a 50 µg/ml stock solution to the *cis* chamber, while 20 µl of a 0.5 mg/ml stock solution was used for the large arrays. The aqueous solution in the chamber consisted of 1.0 M KCl for the 8×8 partition arrays, while a 0.2 M KCl saline solution was used for the large partition arrays. The applied potential across the partition arrays was +60 mV.

The *F. nucleatum* outer membrane protein A (FomA) was kindly provided by Dr. Jörg H. Kleinschmidt (Universität Konstanz, Germany). Incorporation of FomA into established lipid bilayer arrays was carried out by adding 2 µl of refolded FomA (9.6 mg/ml) in *N*-lauryl-*N*,*N*-dimethylammonium-*N*-oxide (LDAO) micelles (LDAO/FomA ratio=800 mol/mol) to the *cis* chamber compartment as previously described [14]. The *cis* and *trans* chamber were filled with a saline solution consisting of 1.0 M KCl, and the applied potential across the partition arrays was +60 mV.

Results and discussion

We created a horizontal biomimetic membrane chamber based on commercially available MatTek glass-bottom culture dishes to make an inexpensive and easily assembled design. Thus, the main chamber parts constitute a disposable single-use biomimetic membrane chamber, where only the custom-designed aluminum sample holder is reusable, and which does not require cleaning prior to re-assembly (Fig. 1).

The design allows for combined optical imaging and voltage-clamp recordings of established bilayers across the micro-structured ETFE LZ200 partition arrays (Fig. 1). The pair of Ag/AgCl electrodes is positioned in the *cis* and *trans* chamber, respectively (Fig. 1b and c). The electrodes therefore give an overall electrical readout of the complete set of membranes established across the micro-structured ETFE LZ200 partition arrays.

The electrical properties of the biomimetic membrane chamber, with non-perforated ETFE LZ200 films, were evaluated. The capacitance (C) and conductance (G) contributions of the chamber setup with non-perforated ETFE LZ200 film were 132±13 pF and 2.5±0.5 nS, respectively. These values of the non-perforated ETFE LZ200 film are defined as the baseline values of C and G.

Establishment of horizontal 8×8 lipid bilayer arrays

Lipid bilayers were established across the micro-structured ETFE LZ200 partition arrays in the horizontal biomimetic membrane chamber by spreading ~0.5 µl of the BFS onto the 8×8 partition array. This resulted in complete lipid membrane coverage of all the partition apertures. In contrast to the previously described establishment of lipid bilayer arrays across vertically positioned ETFE LZ200 partitions [8], the lipid membranes did not thin spontaneously to lipid bilayers in the horizontal setup. In this stage, lipid membranes were stable for days, and could be transported without disrupting the membranes. Manual thinning of lipid membranes was therefore necessary to obtain functional lipid bilayers suitable for insertion of membrane-spanning peptides and proteins. Prior to the manual-thinning process, the deposited membranes were equilibrated for 15 min with the micro-structured ETFE partition. The thinning of the membranes was carried out by gently sweeping a sterile plastic inoculation loop (1 µl capacity) across the entire ETFE partition array. This manual-thinning process took approximately 30 s per array. Repetitions of the sweeping motions across the membranes were required if the bilayer in a single or a few individual apertures ruptured, or if excess BFS flowed back from the surroundings into the actual aperture array positioned in the center of the ETFE partition. The fact that bilayers could be easily re-established if they ruptured during the membrane thinning process resulted in a success rate of ≥98% for establishing bilayers across the partition arrays. The establishment of bilayers in the ETFE arrays could

furthermore be carried out by untrained personnel with no previous experience in establishing black lipid membranes following a short instruction behind the principle of the manual-thinning technique.

To adapt the current manual processes of lipid bilayer formation to a fully automated system for industrial scale applications a robotic deposition technique or a micro fluidic system is envisaged.

The fluorescent lipid analog NBD-PC (1 mol%) included in the BFS provided a convenient visual control over the thinning process, and the Plateau–Gibbs border of the individual bilayers could easily be visualized (Fig. 2).

Following the manual-thinning process, the resulting lipid bilayers were equilibrated for another 15 min in order for the established bilayers to stabilize before carrying out experimentation.

The lipid bilayer arrays established under these conditions had average lifetimes of 1 h with voltage potentials less than or equal to ±100 mV, and exhibited C and G values of 9,750±515 pF and 61±11 nS, respectively. This indicated that the bilayer area constituted around 36–54% of the aperture area [15].

To demonstrate that functional lipid bilayers were established across the horizontal 8×8 arrays the potassium-selective cyclodepsipeptide valinomycin was added to the *cis* chamber to a final concentration of 12 μM [16]. The resulting increase in the current trace recording indicated functional reconstitution of valinomycin, which could effectively be reversed by the addition of the channel blocker TEA (Fig. 3a). This strongly suggested that functional lipid bilayers were established in the horizontal setup.

Sensitivity of current trace recordings of membrane molecules

The current noise increases strongly with the aperture diameters and the recording bandwidth [17]. This could affect the ability to resolve low-conductance events by voltage-clamp recordings in the bilayers established across the horizontal 8×8 partition arrays.

The current noise of the bilayers established in 8×8 arrays was determined to be in the range 3–5 pA peak-to-peak with a frequency bandwidth of 50 Hz. This scale of current noise would be expected to be acceptable for resolving low-conductance events of a wide range of membrane-spanning peptides and proteins, provided that the experimental conditions are optimal (e.g., ionic strength) for the given peptide or protein. We therefore addressed the sensitivity of the bilayers established in the 8×8 partition arrays by incorporating biotechnological or physiological relevant membrane peptides and proteins (Table 1).

The well-characterized peptide gA from *B. brevis* is a cation-selective channel formed by transbilayer association of pentadecapeptide subunits residing in each monolayer of the lipid bilayer [18]. We reconstituted gA into established bilayers by adding gA dissolved in ethanol to both the *cis* and *trans* bilayer chambers. Reconstituted gA peptides exhibited a high channel activity, where multiple gA channel opening and closures could be observed during the current trace (Fig. 3b). The current of single-channel activity with the chosen experimental conditions was expected to be ~20 pA [19]. Channel events with these current values could be distinguished in the current traces

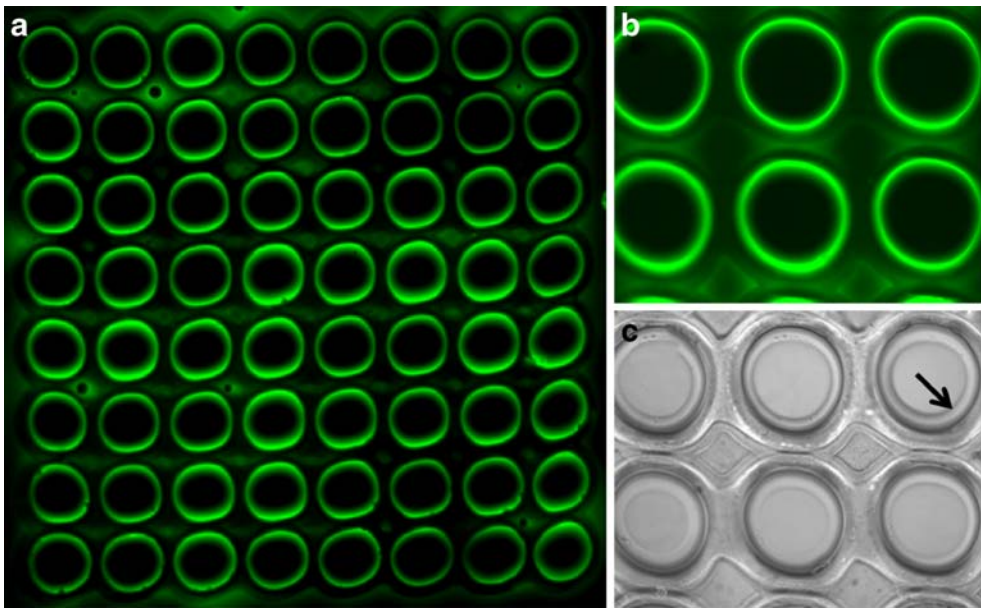

Fig. 2 Fluorescent and bright-field images of established horizontal 8×8 bilayer arrays. **a** Fluorescent image of established 8×8 bilayer array with 25 mg/ml DPhPC in *n*-decane doped with NBD-PC (1 mol%). Image was acquired with a 2.5× air-corrected objective. **b** Fluorescent image acquired with a 10× air-corrected objective, and **c** the corresponding brightfield image. Indicated is the visual appearance of the Plateau–Gibbs border (*black arrow*)

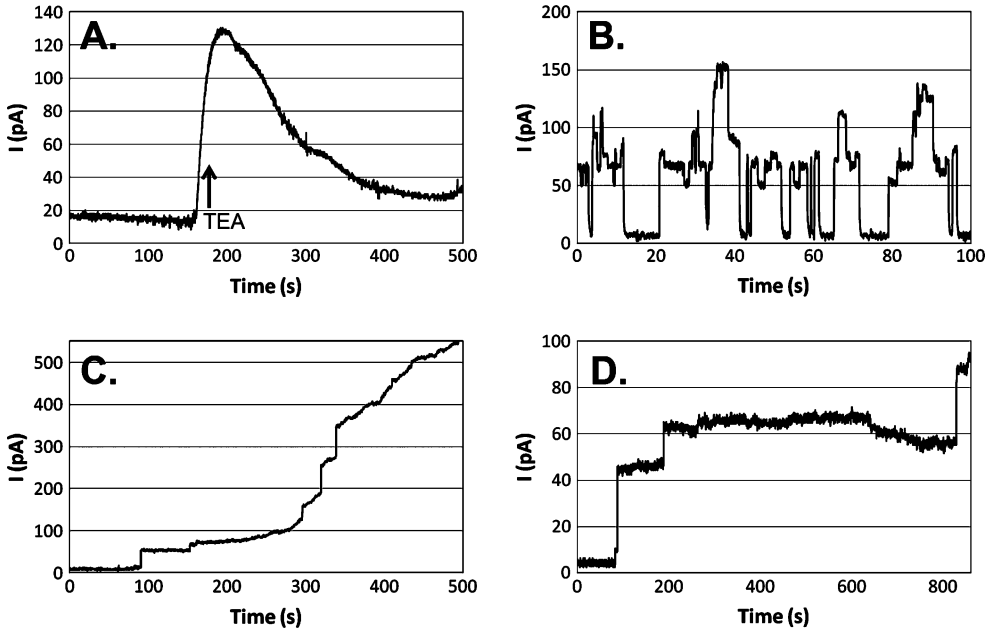

Fig. 3 Current traces of reconstituted membrane peptides and proteins in established 8×8 bilayer arrays. **a** Insertions of valinomycin and blocking by TEA. TEA was added (t=180 s) when the current increased as a consequence of functional valinomycin insertions. **b** Traces of gA channel activities. High channel activities are seen during the current trace with simultaneous opening and closure of multiple channels. Single-channel opening and closure could be distinguished with current values of ~20 pA **c** Reconstitution of heptameric α-HL pores. Single-channel incorporations had current values of ~35 pA. **d** Incorporation of trimeric FomA porins. Single-channel events had current values of approximately 15 pA. In the current traces of **b**, **c**, and **d** multiple insertions together with single-channel events could be observed. Applied potentials were +60 mV in **a**, **c**, and **d** and +150 mV in **b**

of incorporated gA peptides, although with some conductance heterogeneity (Fig. 3b).

We next evaluated the compatibility of the horizontal bilayers in the 8×8 arrays to support functional incorporation of membrane proteins, and to further characterize the ability to resolve low-conductance events. The pore-forming heptameric α-HL membrane protein from *S. aureus* and the trimeric outer-membrane-embedded porin FomA from *F. nucleatum*, respectively, were reconstituted into bilayers established across the partition arrays. The α-HL pores incorporated into the membranes with single-channel currents of around 35 pA (Fig. 3c), agreeing with previous reports [12]. The voltage-dependent FomA channel porins inserted into the membrane with a current of approximately 15 pA (Fig. 3d), which also agreed with previously published current traces [14, 20]. Simultaneous multiple-channel insertions were also observed in the current traces of both reconstituted α-HL pores and FomA channel porins (Fig. 3c and d).

These results show that the bilayers established in the micro-structured 8×8 ETFE LZ200 partitions support low-current (high sensitivity) recordings.

The individual bilayers are, at present, not electrically addressable. Recent approaches have been described that conveniently allow the integration of a membrane scaffold with planar addressable microelectrode arrays [21, 22]. Further developments of the horizontal biomimetic membrane design could therefore be to develop composite membrane scaffolds enabling the electrical readout of individual bilayers. The lipid bilayers are however optically

Table 1 Potential applications of selected membrane peptides and proteins

Name	Type	Biotechnology/pharmacology	References
Valinomycin	Cyclodepsipeptide	Biomedical devices	[30, 31]
gA	Peptide	Sensors for drug-induced toxicity, chemical and biochemical analytes, pH and ammonium	[6, 32–34]
α-HL	Protein	Stochastic sensing techniques	[35, 36]
		Polynucleotide detection and sequencing	[37–41]
FomA	Protein	Drug discovery in Gram-negative bacteria infectious diseases	[42, 43]
		Immunological assays	[44]

individually addressable and fluorescent-based techniques may be combined with the membrane design in order to characterize specific interactions with membrane peptides or proteins [23, 24]. Moreover, the aperture array geometry (diameters of 300 µm and nominal center-to-center distances of 400 µm) provides a platform that may be adapted to modern array scanners and/or automated imaging and image analysis systems.

Lipid bilayers across rectangular 24×24 and hexagonal 24×27 partition arrays

The scalability of the array size is a key feature in the successful development of biotechnological applications based on planar biomimetic membranes. We therefore addressed the scalability of our design by scaling up the partition array size from the 8×8 rectangular arrays to 24×24 rectangular and 24×27 hexagonal EFTE LZ200 partition arrays. The total aperture areas were 0.41 cm^2 for the 24×24 rectangular and 0.45 cm^2 for the 24×27 hexagonal arrays, corresponding to a nine- and ten times area increase, respectively, compared to the 8×8 partition arrays (0.045 cm^2).

Lipid bilayers could be established across the large ETFE LZ200 partition arrays in a similar manner as for the 8×8 partition arrays. Modifications were that 5 µl BFS was needed to cover the large partition arrays and an equilibration period of approximately 1 h were required prior to the membrane thinning to obtain stable membranes. In order to obtain a full view of the bilayers established across the large partition arrays, mosaics of twelve images were assembled for each large array (Fig. 4a and b). The membranes could be evenly thinned across the whole partition array as evidenced by the separate bright appearance of the torus of the

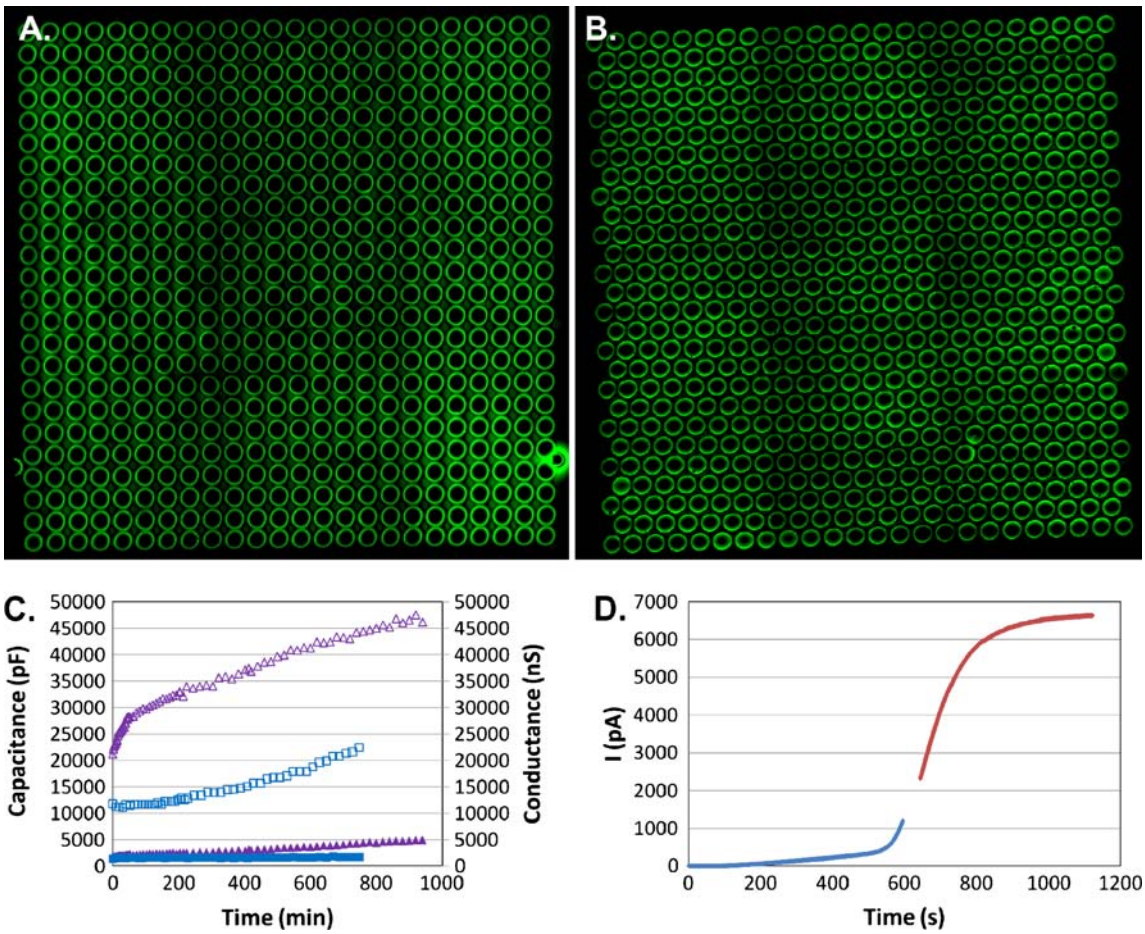

Fig. 4 Comparison of 24×24 rectangular and 24×27 hexagonal bilayer arrays. **a** and **b** Mosaics comprising 12 fluorescent images of the 24×24 rectangular and 24×27 hexagonal bilayer arrays. **c** Capacitance (*open boxes*) and conductance (*filled boxes*) values during the membrane lifetime of the 24×24 rectangular (*purple*) and 24×27 hexagonal (*blue*) arrays. Time=0 is subsequent a 15 min equilibration period after the manual thinning process. **d** Demonstration of α-HL incorporation into a 24×24 rectangular array. The initial amplifier gain was set to 10× (*blue line*). When the amplifier saturated due to the incorporation of α-HL pores, the gain was adjusted and the trace recording was resumed (*red line*). The aqueous solution in the horizontal bilayer chamber consisted of a 0.2 M KCl. The applied potential was +60 mV

individual bilayers (Fig 4a and b). Although the large arrays also needed initial manual thinning, they spontaneously continued the thinning process (Fig 4c). The maximum capacitance values that could be achieved were around 50,000 pF for the 24×24 rectangular arrays, while considerably lower values were obtainable for the 24×27 hexagonal arrays (Fig. 4c).

The bilayers exhibited relatively stable conductance values ranging between 2,000–5,000 nS, depending on the array type, throughout the bilayer lifetimes, indicating good sealing properties of the large arrays (Fig. 4c).

The current noise of the bilayers established across the large arrays was also assessed, and determined to be in the range of 10–20 pA peak-to-peak for both the 24×24 rectangular and the 24×27 hexagonal arrays, respectively.

Surprisingly, the bilayers established across the large partition arrays were considerably more stable than the bilayers established across the 8×8 partition arrays with membrane lifetimes up to around 16 h for both the rectangular and hexagonal arrays. The reason might be that bilayer breakages often appeared at the edges of the partition array. The percentage of bilayers residing at the edges is ~44% for the 8×8 partition arrays, whereas this fraction only constitutes ~16% for the 24×24 arrays and ~15% for the 24×27 arrays, respectively.

To evaluate the functionality of the large bilayer arrays, α-HL was reconstituted into the large arrays (Fig. 4d). The α-HL incorporated exponentially exhibiting a sigmoid current shape, indicating that α-HL incorporated into the bilayers in a cooperative manner (Fig 4d). The large arrays therefore comprised functional bilayers suitable for incorporation of membrane proteins, preferentially in large scale amounts.

Although evenly thinned bilayers could be consistently obtained across the large partition arrays, the spontaneous thinning process varied between experiments. This could mainly be attributed to the manual handling involved in the establishment of the lipid arrays.

To establish large scale biomimetic membrane arrays in a more reproducible manner, an automation technique needs to be integrated with the current horizontal setup. The automation of bilayer formations can be integrated with the horizontal design by either a robotic-based membrane deposition technique or a micro fluidic-based system.

In this study, we have addressed the electro-physical properties of the micro-structured membrane scaffold and the scalability of the bilayer arrays in the constructed horizontal design.

The transportation robustness of the functional bilayer arrays has not been addressed here. However, the thick precursor membranes could be stored and transported without disrupting the membranes in the stage prior to the manual thinning of membranes to lipid bilayers. Encapsulation of the suspended bilayers would be an expected requirement. Recent advantages in bilayer encapsulation methods suggest that a robust portable artificial membrane platform may be produced [25–29].

We conclude that the electro-physical properties of the micro-structured membrane scaffold combined with the scalability of array sizes enable further development of novel biomimetic membrane-based biosensing devices.

Acknowledgments We thank Dr. Jörg H. Kleinschmidt (Universität Konstanz, Germany) for the delivery and guidance with the handling and incorporation of FomA porins. The work was supported through MEMBAQ, a Specific Targeted Research Project (STREP), by the European Commission under the Sixth Framework Program (NMP4-CT-2006-033234), by The Danish National Advanced Technology Foundation (023-2007-1), and The Danish National Research Foundation.

References

1. Suzuki H, Takeuchi S (2008) Anal Bioanal Chem 391:2695–2702
2. Fang Y, Frutos AG, Lahiri J (2002) J Am Chem Soc 124:2394–2395
3. Fang Y, Hong Y, Webb B et al (2006) MRS bulletin 31:5
4. Fang Y, Lahiri J, Picard L (2003) Drug Discov Today 8:755–761
5. Kaczorowski GJ, McManus OB, Priest BT et al (2008) J Gen Physiol 131:399–405
6. Lundbaek JA (2008) J Gen Physiol 131:421–429
7. Vogel J, Perry M, Hansen JS et al (2009) J Micromech Microeng 19:025026
8. Hansen JS, Perry M, Vogel J et al (2009) J Micromech Microeng 19:025014
9. Mueller P, Rudin DO (1969) Curr Topics Bioenergetics 3:157–249
10. Inagaki N, Narushima K, Lim SK, Park YW, Ikeda Y (2002) Journal of Polymer Science Part B: Polymer Physics 40:2871–2882
11. Y. W. Park N I (2004) Journal of Applied Polymer Science 93:1012-1020
12. Hemmler R, Bose G, Wagner R et al (2005) Biophys J 88:4000–4007
13. Wilburn JP, Wright DW, Cliffel DE (2006) Analyst 131:311–316
14. Pocanschi CL, Apell HJ, Puntervoll P et al (2006) J Mol Biol 355:548–561
15. Benz R, Frohlich O, Lauger P et al (1975) Biochim Biophys Acta 394:323–334
16. Stark G, Benz R, Pohl GW et al (1972) Biochim Biophys Acta 266:603–612
17. Mayer M, Kriebel JK, Tosteson MT et al (2003) Biophys J 85:2684–2695
18. Andersen OS, Koeppe RE 2nd (2007) Annu Rev Biophys Biomol Struct 36:107–130
19. Mobashery N, Nielsen C, Andersen OS (1997) FEBS Lett 412:15–20
20. Kleivdal H, Benz R, Jensen HB (1995) Eur J Biochem 233:310–316
21. Baaken G, Sondermann M, Schlemmer C et al (2008) Lab Chip 8:938–944
22. Lin Z, Takahashi Y, Kitagawa Y et al (2008) Anal Chem 80:6830–6833
23. Hebert TE, Gales C, Rebois RV (2006) Cell Biochem Biophys 45:85–109
24. Lohse MJ, Bunemann M, Hoffmann C et al (2007) Curr Opin Pharmacol 7:547–553

25. Jeon TJ, Malmstadt N, Schmidt JJ (2006) J Am Chem Soc 128:42–43
26. Kang XF, Cheley S, Rice-Ficht AC et al (2007) J Am Chem Soc 129:4701–4705
27. Malmstadt N, Jeon J, Schmidt J (2008) Advanced Materials 20:84–89
28. Oliver AE, Kendall EL, Howland MC et al (2008) Lab Chip 8:892–897
29. Uto M, Araki M, Taniguchi T et al (1994) Analytical Sciences 10:943–946
30. Frant MS, Ross JW Jr (1970) Science 167:987–988
31. Schar-Zammaretti P, Ziegler U, Forster I et al (2002) Anal Chem 74:4269–4274
32. Capone R, Blake S, Restrepo MR et al (2007) J Am Chem Soc 129:9737–9745
33. Borisenko V, Zhang Z, Woolley GA (2002) Biochim Biophys Acta 1558:26–33
34. Nikolelis DP, Siontorou CG (1996) Anal Chem 68:1735–1741
35. Braha O, Gu LQ, Zhou L et al (2000) Nat Biotechnol 18:1005–1007
36. Gu LQ, Braha O, Conlan S et al (1999) Nature 398:686–690
37. Ashkenasy N, Sanchez-Quesada J, Bayley H et al (2005) Angew Chem Int Ed Engl 44:1401–1404
38. Kasianowicz JJ, Brandin E, Branton D et al (1996) Proc Natl Acad Sci U S A 93:13770–13773
39. Kasianowicz JJ, Henrickson SE, Weetall HH et al (2001) Anal Chem 73:2268–2272
40. Vercoutere WA, Winters-Hilt S, DeGuzman VS et al (2003) Nucleic Acids Res 31:1311–1318
41. Winters-Hilt S, Vercoutere W, DeGuzman VS et al (2003) Biophys J 84:967–976
42. Bolstad AI, Jensen HB, Bakken V (1996) Clin Microbiol Rev 9:55–71
43. Jensen HB, Skeidsvoll J, Fjellbirkeland A et al (1996) Microb Pathog 21:331–342
44. Guo M, Han YW, Sharma A et al (2000) Oral Microbiol Immunol 15:119–123